Chaos-Based Random Sampling for Photometric Invariant Shoe Detection With Vision Sensor in Human–Robot Coexisting Environments

Pritam Paral, Amitava Chatterjee, *Senior Member, IEEE*, and Anjan Rakshit

***Abstract*—People-following in a leader-follower scheme is considered as a major contemporary research problem in the domain of human-robot coexistence. The problem essentially requires human detection and tracking, and, in recent times, vision sensing based shoe detection has evolved as an effective mechanism for human detection. The problem gets more challenging when the environment becomes affected by photometric conditions like varying illumination, shadows, specularities, etc. Recently, a state-of-the-art fast image template matching algorithm, called *photometric-invariant CFAsT-match (PICFAsT-match)*, has been specifically proposed for shoe detection based people-following in those challenging environments. In this approach, for determining the best shoe matching result corresponding to a frame, each single transformation included in a number of specified grids of general affine transformations is evaluated. However, in order to achieve a high speed real-life implementation of PICFAsT-match, every transformation is assessed by considering a handful number of pixels sampled randomly from the images. Research beyond PICFAsT-match reveals that the matching accuracy significantly relies on the quality of the random sampling. In this paper, we propose an improved variant of PICFAsT-match, called *chaos based PICFAsT-match (CBPICFAsT-match)*, where a novel approach for this process of random sampling of pixels has been developed. This strategy is based on the state-time histories of multiple fractional order chaotic systems. Experimental results aptly demonstrate the superiority of the proposed algorithm, when compared to competing state-of-the-art algorithms, successfully employed for the said shoe detection purpose in human-robot coexisting environments.**

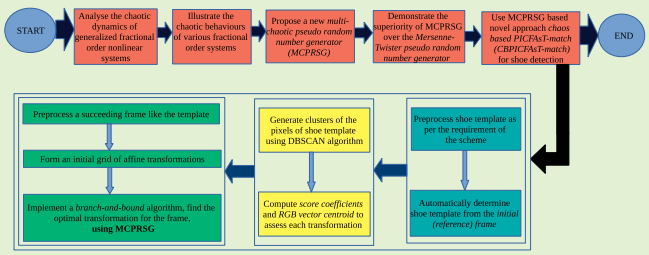

Fig: Overall framework of our proposed *chaos based photometric-invariant CFAsT-match (CBPICFAsT-match)* algorithm

***Index Terms*—Human-robot coexistence, shoe detection, vision sensing, fractional order chaotic systems, multi chaotic pseudo random number generator, photometric-invariant CFAsT-match, chaos based photometric-invariant CFAsT-match.**

I. Introduction

THE problems of following people under motion in human-robot coexisting environments have attracted great attention over the recent years. The main objective for such schemes is to develop a robust and accurate tracking scheme, that will form the core of a *leader-follower* module, where the human will be the leader and the robot will follow the human as well as will perform various assistive jobs under human direction [1]–[3]. One of the main advantages of developing these types of human following or people tracking schemes is that the same robot can be utilized, in those cases, for a variety of objectives, independent of whether the environment is structured or unstructured, static or dynamic.

The functioning of such approaches for recognizing and following a person in front is usually based on a sensor fusion system [3], [4] which put together the information from various onboard sensors of a mobile robot. However, within this domain, a significant sub-problem is to approximate the positions and orientations of the target person's shoes in consecutive frames captured by the onboard vision sensor (mostly a monocular camera) of a wheeled mobile robot, during people following [3], [5], [6]. As mentioned in [3], there are some valid reasons why the shoes of the target person are preferred as the visual target feature over other human attributes, for examples, face, skin, silhouette etc. Several contemporary, state-of-the art algorithms are proposed in the relevant literature, which deal with such human shoe detection and tracking problems [7], [8].

Our previous works in [5], [6] are based on the consideration that, in the course of pursuit, the shoe poses are subjected to different general transformations, for instances, scales, 2D translations, rotations, or 2D affine transformations. These

Manuscript received October 17, 2019; revised January 21, 2020; accepted January 22, 2020. Date of publication January 27, 2020; date of current version April 16, 2020. This research work was supported by the "VISVESVARAYA PHD SCHEME FOR ELECTRONICS & IT", Ministry of Electronics & IT, Government of India. The associate editor coordinating the review of this article and approving it for publication was Dr. Marko Vauhkonen. *(Corresponding author: Pritam Paral.)*

The authors are with the Department of Electrical Engineering, Jadavpur University, Kolkata 700032, India (e-mail: callinpritam@gmail.com; cha_ami@yahoo.co.in; anjan_rakshit@hotmail.com).

Digital Object Identifier 10.1109/JSEN.2020.2969819

research works [5], [6] have aptly illustrated how we can solve the human shoe detection problem by suitably modifying a general-purpose image template matching problem, where the traditional template matching based on 2D translation is extended to cover other natural transformations, such as, scales, rotations, shears, or 2D affine transformations.

In [5], we had first illustrated the effective implementations of a well-known fast randomized template matching algorithm, named FAsT-match [9], and its modified version in RGB colour domain, named CFAsT-match [10], for identifying human shoes in succeeding frames. But as we had demonstrated in [5], CFAsT-match does not yield reliable outcomes, while detecting human shoes in real-life images (frames) which are subjected to photometric variations, such as illumination, shadows, specularities etc. as well as affected with inadequate brightnesses and contrasts. To overcome the drawbacks of CFAsT-match, we had proposed a novel state-of-the-art variant of it, called *photometric-invariant CFAsT-match* (PICFAsT-match) in [5]. The research work carried out in [5] had implemented both PICFAsT-match and CFAsT-match algorithms for real-life shoe detection in consecutive frames, utilizing DBSCAN [11], known as a popular density based clustering algorithm. In [6], we had demonstrated another approach for solving similar problems of visual target detection, named *OPTICS-based visual target detection (OBVTD)* algorithm, whose implementation was carried out based on OPTICS [12], another density based clustering approach. While considering various challenging real-life scenarios of shoe detection, the PICFAsT-match and OBVTD based implementations could clearly outperform the implementations based on CFAsT-match, as reported in [5], [6].

In case of any of the above algorithms, in order to determine the optimal transformation causing the best matching result corresponding to a frame, we assess each single transformation which belongs to several specified grids of general affine transformations [5]. An individual transformation is evaluated through a *sublinear* estimation [13] of the corresponding *similarity measure* function (e.g. *Colour-Sum-of-Absolute-Differences (CSAD) distance* function [10] in case of CFAsT-match). The sublinear estimation brings down the runtime of the corresponding algorithm in a dramatic fashion, while maintaining the accuracy nearly unaltered. This approximation can potentially be a very crucial factor in real life implementations, because, ideally, the runtime of the algorithm should be very small (in ms order) so that it can be made suitable for detecting and tracking people in real life. The idea is to estimate the similarity measure function by *randomly* scanning only a minor fraction of pixels from the images [13].

However, further research explores that the degrees of uniformity and correlation provided by the random sequences of pixel indices reasonably influence the matching results. The distribution of the pixel indices should have a higher degree of uniformity and lesser degree of correlation so that the accuracy remains virtually unaffected. In our previous CFAsT-match, PICFAsT-match and OBVTD based implementations, for randomly sampling the image pixels, we utilized inbuilt functions of Python's `random` module, which employs the most widely used general purpose pseudo-random number generator (PRNG) called *Mersenne Twister (MT)*, as the core generator [14]. In this paper, a new, more efficient approach for shoe detection problems in human-robot coexisting environments is introduced where we propose to utilize a new pseudo-random sequence generator based on multiple fractional order chaotic systems [15], called *multi-chaotic pseudo-random sequence generator (MCPRSG)* to perform the random selection based operations.

Various chaotic properties, for instance, *sensitive dependence on initial conditions* and *system parameters*, *non-periodicity*, *pseudo-random property*, and *topological transitivity* [15] motivate the researchers to use different chaotic systems for generating pseudo-random sequences [16] which play a pivotal role in various domains, such as, error control coding, *Monte Carlo* simulations in numerical analysis, statistical sampling, etc [17], [18]. Besides, since the chaotic attractors are highly sensitive to their initial conditions and parameters and the degrees of uniformity and independence offered by the chaos based random sequences are sufficiently high, the chaotic systems, in recent times, are being extensively used in cryptography [19], [20]. However, the fractional-order chaotic systems show more abundant dynamic characteristics compared to their integer order counterparts, on account of their *nonlocal* features and severe *nonlinearities* [21], and the degrees of uniformity and independence of the pseudo-random sequences generated with them are further improved. Apart from that, the fractional order chaotic systems can provide a much larger number of pseudo-random sequences along with a more sensitive random number generation process, owing to the fact that the dynamics of the fractional order chaotic systems do not rely only on the initial conditions but also on the fractional derivative orders. It has been shown that, when employed in cryptography [22], [23], the fractional order chaotic systems increase the sizes of the *key spaces* and remarkably improve the security.

Different statistical tests for distribution and independence confirm that the pseudo-random sequences obtained with our proposed MCPRSG offer better degrees of uniformity and independence compared to those generated by MT-PRNG, which leads us to propose an improved variant of PICFAsT-match, called *chaos based PICFAsT-match (CBPICFAsT-match)* in this paper for the shoe detection purposes. Experimental results and performance evaluations carried out for detecting human shoes during people following in human-robot coexisting environments show the supremacy of the proposed algorithm.

The remainder of this paper is organized as follows. Section II presents different stages of the proposed shoe detection approach, in a nutshell. Section III discusses the concepts of fractional calculus and fractional order chaotic systems used in the proposed approach. Section IV briefly describes various fractional order chaotic systems utilized in our proposed pseudo-random number generation scheme. Section V presents our proposed pseudo-random sequence generation scheme based on fractional order chaotic systems. In Section VI, we statistically compare the proposed pseudo-random sequence generator with the Mersenne Twister

Algorithm 1 Computations of Score Coefficient $\Delta\phi$ and RGB Vector Centroid $\mu(\mathcal{I}_1)$ [5]

Input: Colour shoe template $\mathcal{I}_1$

Output:1) Score Coefficient $\Delta\phi$;
2) RGB values $\mu(\mathcal{I}_1)$ of each cluster centroid corresponding to $\mathcal{I}_1$.

STEP-1 Apply the DBSCAN algorithm on $\mathcal{I}_1$ to form arbitrarily shaped clusters of the pixels of $\mathcal{I}_1$.

STEP-2 Determine the total number of clusters $\mathfrak{N}_c$.

STEP-3 Calculate the length of each generated cluster $\mathfrak{l}_m$ ($m = 1, 2, \ldots, \mathfrak{N}_c$). Let the n^{th} element belonging to the m^{th} cluster be indicated by $\mathcal{Y}_{m,n}$.

STEP-4 Calculate $\Delta\phi_m$ and $(\mu(\mathcal{I}_1))_m^l$ ($l = R, G, B$), for each cluster m ($m = 1, 2, \ldots, \mathfrak{N}_c$) as follows:

for $m = 1{:}\mathfrak{N}_c$

$$(\mu(\mathcal{I}_1))_m^l = \frac{\sum_{n=1}^{\mathfrak{l}_m} \mathcal{I}_1^l(\mathcal{Y}_{m,n})}{\mathfrak{l}_m};$$

$$\Delta\phi_m = \frac{1}{\mathfrak{l}_m};$$

end

STEP-5 Return $\Delta\phi$ and $\mu(\mathcal{I}_1)$.

PRNG used in the PICFAsT-match and OBVTD based implementations. Then, the evaluation of the real-life performance of our proposed CBPICFAsT-match is presented in detail in Section VII. Finally, Section VIII concludes the paper.

II. Proposed Shoe Detection Approach

In this paper, we propose a new variant of the earlier proposed PICFAsT-match for the shoe detection in photometrically affected real-life environments, called *chaos based PICFAsT-match (CBPICFAsT-match)*, which is primarily based on multiple fractional order chaotic systems. The proposed approach mainly consists of *three* major phases. Like our earlier proposed approaches in [5], [6], here also we consider the initial frame captured during tracking as the *reference frame* in the CBPICFAsT-match algorithm, which is also the *matching image* in our proposed algorithm. The three phases of the proposed approach are described below.

PHASE-1 At first, by implementing an intelligent algorithm, the target shoes are identified in the matching image, and then, a rectangular *template image* primarily containing the target shoes, is extracted from the matching image [5]. After that, the shoe template, denoted by $\mathcal{I}_1$, is preprocessed, in accordance with the requirements of the proposed scheme [5].

PHASE-2 In this phase, like PICFAsT-match, we utilize the DBSCAN algorithm to generate various arbitrarily shaped clusters of the pixels of the preprocessed template image [5]. Based on the information obtained from different clusters, we compute the parameters score coefficient and RGB vector centroid, denoted by $\Delta\phi$ and μ respectively, which are required to assess the fitnesses of the affine transformations [5]. Algorithm 1 presents the method with which we perform computations of the score coefficient and the RGB vector centroid [5].

PHASE-3 In the final phase, a succeeding frame, denoted by $\mathcal{I}_2$, is considered for matching purpose and the frame is preprocessed in the same way as $\mathcal{I}_1$. Then, we determine the optimal 2D affine transformation which provides the best matching result corresponding to $\mathcal{I}_2$ [5]. A single transformation T in a specified grid $\mathcal{G}_\rho$ (where ρ is a precision parameter) is evaluated through a *sublinear* estimation of the *Adapted-Colour-Sum-of-Absolute-Differences* (ACSAD) distance function $\xi_T(\mathcal{I}_1, \mathcal{I}_2)$ which is considered as the *similarity measure* function in our approach [5]. The mathematical expression of $\xi_T(\mathcal{I}_1, \mathcal{I}_2)$ is available in [5].

$$\xi_T(\mathcal{I}_1, \mathcal{I}_2) = \frac{1}{\upsilon}\sum_{j=1}^{\upsilon} \Upsilon(\mathcal{I}_1(p_j), \mathcal{I}_2(T(p_j))) \tag{1}$$

where,

- $\Upsilon(\mathcal{I}_1(p_j), \mathcal{I}_2(T(p_j)))$
$$= \begin{cases} \Omega(\mathcal{I}_1(p_j), \mathcal{I}_2(T(p_j))) * \Delta\phi(p_j), \\ \quad \text{if}\, \mathfrak{D}\left(\mu\left(\mathcal{I}_1\left(p_j\right)\right), \mathcal{I}_2\left(T(p_j)\right)\right) \le \varrho \\ 1, \ \text{if}\, \mathfrak{D}\left(\mu\left(\mathcal{I}_1\left(p_j\right)\right), \mathcal{I}_2\left(T(p_j)\right)\right) > \varrho \end{cases}$$
- $\Omega(\mathcal{I}_1(p_j), \mathcal{I}_2(T(p_j)))$
$$= \left[\left|\sigma_{\mathcal{I}_1^G}\sigma_{\mathcal{I}_1^B}\right| \left|\mathcal{I}_1^R\left(p_j\right) - \left(\frac{\sigma_{\mathcal{I}_1^R}}{\sigma_{\mathcal{I}_2^R}} \cdot \mathcal{I}_2^R\left(T(p_j)\right)\right) + \varpi_R\right| + \left|\sigma_{\mathcal{I}_1^B}\sigma_{\mathcal{I}_1^R}\right| \left|\mathcal{I}_1^G\left(p_j\right) - \left(\frac{\sigma_{\mathcal{I}_1^G}}{\sigma_{\mathcal{I}_2^G}} \cdot \mathcal{I}_2^G\left(T(p_j)\right)\right) + \varpi_G\right| + \left|\sigma_{\mathcal{I}_1^R}\sigma_{\mathcal{I}_1^G}\right| \left|\mathcal{I}_1^B\left(p_j\right) - \left(\frac{\sigma_{\mathcal{I}_1^B}}{\sigma_{\mathcal{I}_2^B}} \cdot \mathcal{I}_2^B\left(T(p_j)\right)\right) + \varpi_B\right|\right]$$
- $\mathfrak{D}\left(\mu\left(\mathcal{I}_1\left(p_j\right)\right), \mathcal{I}_2\left(T(p_j)\right)\right)$
$$= \left[\left|\sigma_{\mathcal{I}_1^G}\sigma_{\mathcal{I}_1^B}\right| \left|\mu\left(\mathcal{I}_1(p_j)\right)^R - \left(\frac{\sigma_{\mathcal{I}_1^R}}{\sigma_{\mathcal{I}_2^R}} \cdot \mathcal{I}_2^R\left(T(p_j)\right)\right) + \varpi_R\right| + \left|\sigma_{\mathcal{I}_1^B}\sigma_{\mathcal{I}_1^R}\right| \left|\mu\left(\mathcal{I}_1(p_j)\right)^G - \left(\frac{\sigma_{\mathcal{I}_1^G}}{\sigma_{\mathcal{I}_2^G}} \cdot \mathcal{I}_2^G\left(T(p_j)\right)\right) + \varpi_G\right| + \left|\sigma_{\mathcal{I}_1^R}\sigma_{\mathcal{I}_1^G}\right| \left|\mu\left(\mathcal{I}_1(p_j)\right)^B - \left(\frac{\sigma_{\mathcal{I}_1^B}}{\sigma_{\mathcal{I}_2^B}} \cdot \mathcal{I}_2^B\left(T(p_j)\right)\right) + \varpi_B\right|\right]$$

where, for $l = R, G, B$, the variables $\sigma_{\mathcal{I}_1^l}$ and $\sigma_{\mathcal{I}_2^l}$ denote the standard deviations of the sets of pixel values $\{\mathcal{I}_1^l(p_1), \ldots, \mathcal{I}_1^l(p_\upsilon)\}$, and $\{\mathcal{I}_2^l(T(p_1)), \ldots, \mathcal{I}_2^l(T(p_\upsilon))\}$ respectively; $\varpi_l = \left(-\mathcal{M}_{\mathcal{I}_1^l} + \frac{\sigma_{\mathcal{I}_1^l}}{\sigma_{\mathcal{I}_2^l}}\mathcal{M}_{\mathcal{I}_2^l}\right)$; $\mathcal{M}_{\mathcal{I}_1^l}$ and $\mathcal{M}_{\mathcal{I}_2^l}$ indicate the means of the sets of pixel values $\{\mathcal{I}_1^l(p_1), \ldots, \mathcal{I}_1^l(p_\upsilon)\}$, and $\{\mathcal{I}_2^l(T(p_1)), \ldots, \mathcal{I}_2^l(T(p_\upsilon))\}$ respectively; $\mu\left(\mathcal{I}_1(p_j)\right)$ denotes the RGB intensity value of the centroid associated with the cluster containing

Algorithm 2 Evaluation of an Individual Transformation

Input: Colour shoe template $\mathcal{I}_1$, a colour frame $\mathcal{I}_2$, an affine transformation T, a precision parameter α [5], score coefficient $\Delta\phi$, RGB vector centroid $\mu(\mathcal{I}_1)$, likeness threshold ϱ [5].

Output: An approximation ψ_T of the ACSAD distance $\xi_T(\mathcal{I}_1, \mathcal{I}_2)$.

STEP-1 Define a set $\mathbf{V}$ of shoe template pixels actually belonging to various clusters generated by DBSCAN.

STEP-2 Form a set $\mathbf{W}$ of pixels sampled randomly from $\mathbf{V}$ by using the newly proposed MCPRSG which is based on fractional order chaotic systems. The length of the set is considered to be $\mathtt{w} = \Theta(1/\alpha^2)$. The indices of the sampled pixels are obtained as follows:

for j = 1:w

$\mathbf{W}_j = \boldsymbol{\mathcal{B}}_j \cdot \mathcal{X} + \boldsymbol{\mathcal{C}}_j$;

where, $\boldsymbol{\mathcal{B}} = \mathbf{Y}_1|_{\mathcal{S}=2^{k-1}}$, $\boldsymbol{\mathcal{C}} = \mathbf{Y}_2|_{\mathcal{S}=2^k}$, $k = 7$ (preferably), $\mathcal{X}$ = width of the shoe template $\mathcal{I}_1$.

STEP-3 Let the $\mathtt{w}$ number of pixels in $\mathbf{W}$ and corresponding (affine) transformed pixels in $\mathcal{I}_2$ be denoted by $\mathtt{p}_1, \mathtt{p}_2, \ldots, \mathtt{p}_\mathtt{w}$, and $T(\mathtt{p}_1), T(\mathtt{p}_2), \ldots, T(\mathtt{p}_\mathtt{w})$ respectively.

STEP-4 Evaluate $\psi_T = \frac{1}{\mathtt{w}} \sum_{j=1}^{\mathtt{w}} \Upsilon(\mathcal{I}_1(\mathtt{p}_j), \mathcal{I}_2(T(\mathtt{p}_j)))$ with the help of (1).

STEP-5 Return ψ_T.

p_j; $\Delta\phi(p_j)$ is the score-coefficient corresponding to the cluster containing p_j, ϱ is the *likeness threshold* [5].

To perform the sublinear estimation, we have randomly sampled pixels from the images with a newly proposed pseudo-random number generator, named *multi chaotic pseudo-random sequence generator (MCPRSG)*, which is based on the state-time histories of multiple fractional order chaotic systems. The complete procedure of estimating $\xi_T(\mathcal{I}_1, \mathcal{I}_2)$ using MCPRSG is presented in Algorithm 2.

Besides, a *branch-and-bound* scheme [5] is formulated in our implementation, which, despite using the grids of affine transformations with finer resolutions, significantly limits the number of transformations to be evaluated in the rapidly evolving nets. The runtime of the CBPICFAsT-match algorithm gets further curtailed with the introduction of this formulation. The branch-and-bound algorithm associated with CBPICFAsT-match is depicted in the form of a flow chart in Fig. 1 [5].

Now, it is worthy to mention that, with the shoe template $\mathcal{I}_1$ available, the CBPICFAsT-match algorithm can then be implemented again and again for the subsequent frames captured, and thus, our proposed algorithm is made competent for tracking humans in real-life [5].

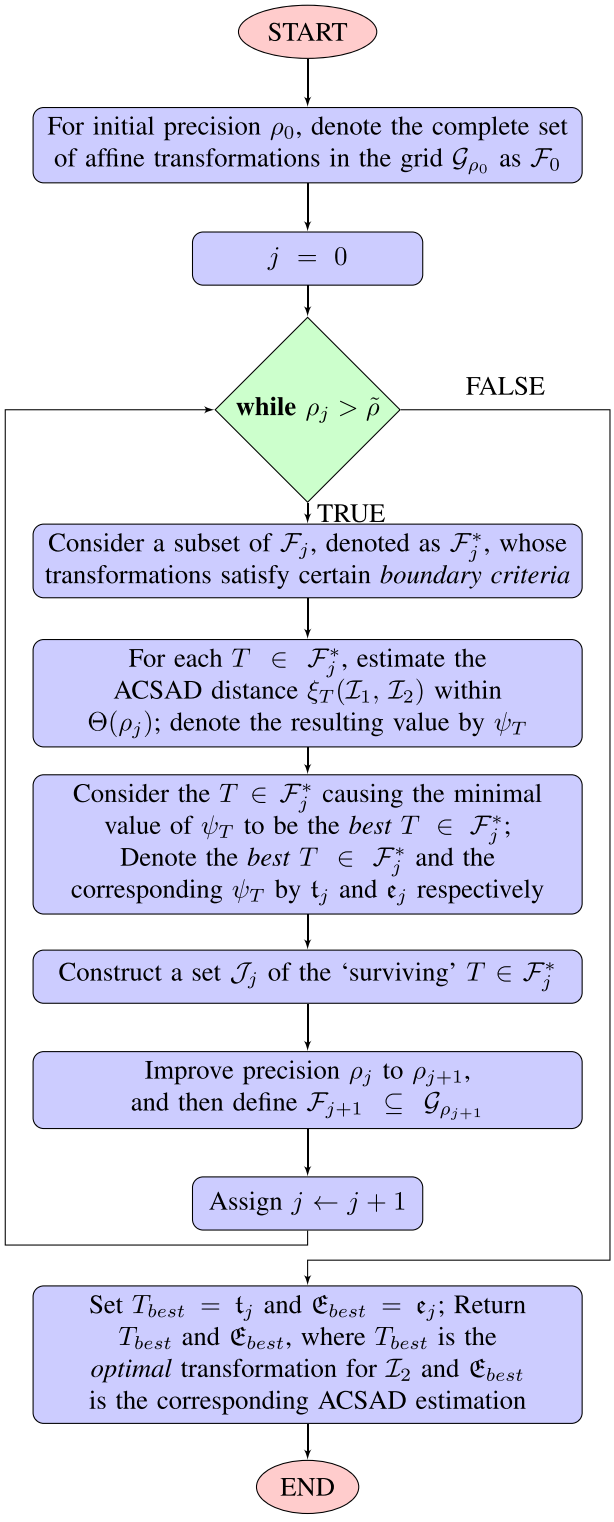

Fig. 1. Flowchart of the *branch-and-bound* algorithm [5].

III. Concepts of Fractional Calculus and Fractional Order Chaotic Systems (FOCHS) Used in the Proposed Approach

For generating pseudo-random sequences in our proposed approach, we have utilized the state-time histories of various fractional order chaotic systems, which are computed by using the popular *Grünwald–Letnikov* (G-L) definition [15] and the *short-memory principle* [24] of fractional calculus. To the best of our knowledge and belief, this is the first work which demonstrates a successful real-life application of these concepts for shoe detection problems. Here, we will briefly discuss the G-L definition and the short-memory principle.

Also, we will briefly illustrate the dynamics of generalized fractional order nonlinear systems for exhibiting chaos.

A. Grünwald–Letnikov Fractional Differintegral

At least 15 various definitions of fractional order derivatives and integrals (known as 'differintegrals' in short) have so far been proposed in the domain of fractional calculus [15]. However, among those, the most widely used definition to perform effective numerical computations is the Grünwald–Letnikov (G-L) definition, which is also utilized in this paper. The G-L definition is based on the principle of generalization of the *successive differentiations*. The n-th order derivative of the function $g(t)$ by t (where $n \in \mathbb{N}$, $i > n$) is defined as [15]

$$\mathcal{D}_t^n g(t) = \underset{h\to 0}{Lt} \left(\frac{1}{h^n}\right) \sum_{i=0}^{n} \left[(-1)^i \binom{n}{i} g(t-ih)\right], \quad \text{where,}$$

$$\binom{n}{i} = \frac{n!}{i!\,(n-i)!} = \frac{\Gamma(n+1)}{\Gamma(i+1)\,\Gamma(n-i+1)}.$$

When we generalize the mathematical expression of the n-th order derivative for $n = \delta$ (where $\delta \in \mathbb{R}^+$), we obtain

$${}_\beta\mathcal{D}_t^\delta g(t) = \underset{h\to 0}{Lt} \left(\frac{1}{h^\delta}\right) \sum_{i=0}^{\lfloor \frac{t-\beta}{h} \rfloor} \left[(-1)^i \binom{\delta}{i} g(t-ih)\right], \quad (2)$$

where, $(-1)^i \binom{\delta}{i}$, $i = 0, 1, 2, \cdots$ indicate the fractional order binomial coefficients which are calculated based on the relation between *Gamma* function and factorial. Further, we denote $(-1)^i \binom{\delta}{i}$ as $\mathcal{A}_i^\delta$ for $i = 0, 1, 2, \cdots$, which can be recursively computed by making use of the following relations

$$\mathcal{A}_0^\delta = 1, \quad \mathcal{A}_i^\delta = \left(1 - \frac{1+\delta}{i}\right) \mathcal{A}_{i-1}^\delta. \quad (3)$$

B. Implementation of the Short-Memory Principle

It is worth mentioning that, when we numerically compute the fractional differintegrals or solve various fractional order differential equations by using the G-L definition in (2), the corresponding computational costs are quite heavy. This is due to the fact that, in order to calculate any fractional differintegral, we require to compute the complete history of the function at each point, which is irrelevant to its integer order counterpart on account of being local operation. For example, based on (2), the numerical solution of a simple fractional order homogeneous differential equation, such as $\mathcal{D}^\delta v(t) + c\, v(t) = 0$ becomes as complex as

$$v(wh) = -ch^\delta v(wh-h) - \sum_{i=1}^{w} \mathcal{A}_i^\delta v(wh-ih). \quad (4)$$

for $w = r, r+1, \cdots$, and h is a considerably small step size. So, if t goes on increasing, we will have to compute more and more number of terms to find the solution. To overcome this constraint, the *short memory principle* of fractional calculus [24] can be utilized, where the summation is shortened to some extent in accordance with the accuracy requirement. The truncation of the summation will introduce an insignificant amount of error in the solution, since the distant past of the function $v(t)$ has a negligible effect on the calculation of the G-L derivative. However, the method will significantly reduce the computational burden.

When employed in the computation of (4), the short memory principle defines a memory length N_m and the lower limit of the summation is altered to $i = \vartheta$ with the following rule,

$$\vartheta = \begin{cases} 1 & \text{for } i \le \dfrac{N_m}{h} \\ \left\lfloor i - \dfrac{N_m}{h} \right\rfloor & \text{for } i > \dfrac{N_m}{h}. \end{cases}$$

We can ensure an accuracy of γ by properly selecting N_m as

$$N_m \ge \left(\frac{\mathcal{U}}{\gamma\, |\Gamma(1-\delta)|}\right)^{1/\delta},$$

while $\mathcal{U}$ is an upper bound of $v(t)$.

C. Dynamics of Fractional Order Chaotic Systems

We often represent a fractional order chaotic system by the generalized incommensurate order fractional nonlinear system which can be written as follows [15]:

$$\begin{aligned} {}_0\mathcal{D}_t^{\delta_j} x_j(t) &= F_j(x_1(t), x_2(t), \ldots, x_n(t), t), \\ x_j(0) &= a_j, \quad j = 1, 2, \ldots, n, \end{aligned} \quad (5)$$

where a_j are the initial conditions.

The vector representation of (5) has the following form:

$$\mathcal{D}^{\boldsymbol{\delta}} \mathbf{x} = \mathbf{F}(\mathbf{x}) \quad (6)$$

where $\boldsymbol{\delta} = [\delta_1, \delta_2, \ldots, \delta_n]^T$ for $0 < \delta_j < 2$, $(j = 1, 2, \ldots, n)$ and $\mathbf{x} \in \mathbb{R}^n$.

The equilibrium points corresponding to the system (6) are computed by solving the following equation

$$\mathbf{F}(\mathbf{x}) = 0 \quad (7)$$

and it is supposed that $\hat{\mathcal{E}} = (\hat{x_1}, \hat{x_2}, \ldots, \hat{x_n})$ is an equilibrium point of system (6).

Now, in order to analyze the chaotic behaviour of the fractional order nonlinear system (6), we need to evaluate the Jacobian matrices of the system (6) $\mathbf{J} = \partial\mathbf{F}/\partial\mathbf{x}$ (where $\mathbf{F} = [F_1, F_2, \ldots, F_n]^T$) at different equilibrium points calculated for certain parameter values. Once the Jacobian matrices are obtained, the eigenvalues for different equilibrium points are computed using the following characteristic equation

$$\det(\lambda \mathbf{I} - \mathbf{J}_{\hat{\mathcal{E}}}) = 0. \quad (8)$$

where λ are all eigenvalues of the Jacobian matrix $\mathbf{J}_{\hat{\mathcal{E}}}$ evaluated at equilibrium $\hat{\mathcal{E}}$.

With the eigenvalues λ, we can easily determine the nature of the equilibrium points. For example, when all eigenvalues are real in nature and at least one of them is positive (unstable) and at least one is negative (stable), an equilibrium $\hat{\mathcal{E}}$ is considered to be a *saddle point*. The saddles are inherently unstable. The necessary condition for the system (6) to exhibit chaos is keeping at least one eigenvalue in the *unstable* region.

1) Stability Condition for Commensurate Orders: For $\delta_1 = \delta_2 = \cdots \delta_n \equiv \delta$, the equilibrium points are asymptotically stable if all the eigenvalues λ_j $(j = 1, 2, \ldots, n)$ of the $\mathbf{J}$, evaluated at $\hat{\mathcal{E}}$, satisfy the following condition [15]:

$$|\arg(\text{eig}(\mathbf{J}_{\hat{\mathcal{E}}}))| = |\arg(\lambda_j)| > \delta\frac{\pi}{2}, \quad j = 1, 2, \ldots, n \tag{9}$$

With unstable eigenvalues $\lambda_{1,2} = \mathcal{P}_{1,2} \pm j\mathcal{Q}_{1,2}$, the minimum commensurate order for which a nonlinear system can generate chaos is calculated as follows [15]:

$$\delta > \frac{2}{\pi}\text{atan}\left(\frac{|\mathcal{Q}_i|}{\mathcal{P}_i}\right), \quad i = 1, 2 \tag{10}$$

2) Stability Condition for Incommensurate Orders: Let us consider the incommensurate real derivative orders $\delta_1 \neq \delta_2 \neq \cdots \neq \delta_n$, where $\delta_j = w_j/v_j$; $w_j, v_j \in \mathbb{Z}^+$ for $j = 1, 2, \ldots, n$. Now, if we assign $\varepsilon = 1/p$, where p indicates the LCM of the denominators v_j, the characteristic equation of the system (6) corresponding to the Jacobian matrix $\mathbf{J}_{\hat{\mathcal{E}}}$ becomes:

$$\det(\text{diag}([\lambda^{p\delta_1}\lambda^{p\delta_2}\cdots\lambda^{p\delta_n}]) - \mathbf{J}_{\hat{\mathcal{E}}}) = 0 \tag{11}$$

and then the condition of stability is given as follows [15]:

$$|\arg(\lambda_j)| > \varepsilon\frac{\pi}{2} \tag{12}$$

for all eigenvalues λ_j.

The necessary condition for the system (6) to exhibit chaotic behaviour will get satisfied if the characteristic equation given in (11) has at least one unstable root. This is possible if the condition $|\arg(\lambda)| < \pi/2p$ holds true.

IV. Brief Descriptions of Various Fractional Order Chaotic Systems

In this section, we will discuss various fractional order chaotic systems on which our proposed pseudo-random sequence generator is based.

A. Fractional Order Rössler's System

The Rössler's attractor was originally proposed by Otto Rössler in 1976. Its fractional order generalization is considered as follows [15]:

$$\begin{aligned} {}_0\mathcal{D}_t^{\delta_1}x_1(t) &= -(x_2(t) + x_3(t)),\\ {}_0\mathcal{D}_t^{\delta_2}x_2(t) &= x_1(t) + ax_2(t),\\ {}_0\mathcal{D}_t^{\delta_3}x_3(t) &= b + x_3(t)(x_1(t) - c), \end{aligned} \tag{13}$$

where δ_1, δ_2, δ_3 are the fractional derivative orders and a, b, c are parameters.

We consider (13) with the parameters $a = 0.5$, $b = 0.2$ and $c = 10$. For these parameter values, we get two *unstable* equilibria $\mathcal{E}_1$ and $\mathcal{E}_2$ as reported in Table I and thus, the condition for demonstrating chaotic behaviour gets satisfied.

Now, when we assume the fractional commensurate orders $\delta_1 = \delta_2 = \delta_3 = 0.9$ $(\delta > 0.839)$ and the same system parameters $a = 0.5$, $b = 0.2$, $c = 10$, we obtain an unstable root $\lambda_1 \approx 0.9208$ by solving the characteristic equation for $\mathcal{E}_1$. Also, from the characteristic equation corresponding to $\mathcal{E}_2$, we find the unstable roots $\lambda_{1,2} \approx 0.9892 \pm 0.1460j$, as $|\arg(\lambda_{1,2})| = 0.1466 < 0.9\frac{\pi}{2}$. Hence, the chaotic behaviour of system (13) gets confirmed, in accordance with (9).

B. Fractional Order Volta's System

The Volta's system was invented in 1984 by Volta who was in the Department of Physics, Genova University. The fractional order Volta's system is described as follows [15]:

$$\begin{aligned} {}_0\mathcal{D}_t^{\delta_4}x_4(t) &= -x_4(t) - ax_5(t) - x_6(t)x_5(t)),\\ {}_0\mathcal{D}_t^{\delta_5}x_5(t) &= -x_5(t) - bx_4(t) - x_4(t)x_6(t),\\ {}_0\mathcal{D}_t^{\delta_6}x_6(t) &= cx_6(t) + x_4(t)x_5(t) + 1, \end{aligned} \tag{14}$$

where δ_4, δ_5, δ_6 are the fractional derivative orders and a, b, c are system parameters.

For the parameters $a = 19$, $b = 11$ and $c = 0.73$, the system described by (14) has three *unstable* equilibria $\mathcal{E}_1$, $\mathcal{E}_2$ and $\mathcal{E}_3$ as mentioned in Table I and hence, chaos can be observed.

Now, if we assume the fractional commensurate orders $\delta_4 = \delta_5 = \delta_6 = 0.98$ $(\delta > 0.977)$ along with the same system parameters $a = 19$, $b = 11$, $c = 0.73$, we obtain a pair of unstable roots $\lambda_1 \approx 0.9968$ and $\lambda_2 \approx 1.0257$ from the characteristic equation corresponding to $\mathcal{E}_1$, whereas solving the characteristic equation for $\mathcal{E}_2$ yields the unstable roots $\lambda_{1,2} \approx 1.0240 \pm 0.0160j$, as $|\arg(\lambda_{1,2})| = 0.0157 < 0.98\frac{\pi}{2}$. Also, an unstable root $\lambda_1 \approx 1.0214$ can be found by solving the characteristic equation for $\mathcal{E}_3$. Therefore, we can confirm the chaotic behaviour of (14), in accordance with (9).

C. Fractional Order Lü's System

In the study of chaos theory, the Lü's system is considered as a connector between the so-called Lorenz's system and Chen's system. Its fractional order version is defined as [15]:

$$\begin{aligned} {}_0\mathcal{D}_t^{\delta_7}x_7(t) &= a(x_8(t) - x_7(t)),\\ {}_0\mathcal{D}_t^{\delta_8}x_8(t) &= -x_7(t)x_9(t) + cx_8(t),\\ {}_0\mathcal{D}_t^{\delta_9}x_9(t) &= x_7(t)x_8(t) - bx_9(t), \end{aligned} \tag{15}$$

where δ_7, δ_8, δ_9 are the fractional derivative orders and a, b, c are parameters.

The system (15) is considered with the parameters $a = 36$, $b = 3$ and $c = 20$. For these parameter values, we obtain three *unstable* equilibria $\mathcal{E}_1$, $\mathcal{E}_2$ and $\mathcal{E}_3$ as reported in Table I and thus, the condition for observing chaos gets satisfied.

Now, let us assume the incommensurate derivative orders $\delta_7 = 0.985$, $\delta_8 = 0.99$, $\delta_9 = 0.98$ $(\delta > 0.9156)$ and the same system parameters, given as, $a = 36$, $b = 3$, $c = 20$. With these orders and parameters, we get unstable roots λ (as $|\arg(\lambda)| < \pi/2p$, where $p = 1000$) from the characteristic equations corresponding to $\mathcal{E}_1$, $\mathcal{E}_2$ and $\mathcal{E}_3$ individually, and thus, the condition for chaotic behaviour of the system (15) gets satisfied in accordance with (12).

V. Proposed Multi Chaotic Pseudo Random Sequence Generator

It is worth-mentioning that the arrays of state-time history are of 64-*bit floating point* data-type. A number of this data-type, on an average, can contain about 14 to 15 digits after the decimal point. Considering these facts, we generate

TABLE I
CHAOTIC BEHAVIOURS OF VARIOUS FRACTIONAL ORDER SYSTEMS

Fractional Order Chaotic Systems	Locations of the Equilibrium Points	Corresponding Eigenvalues	Natures of the Equilibrium Points	Minimal Com -mensurate Order (δ)
Rössler's System	$\mathcal{E}_1 = (9.98998; -19.97997; 19.97997)$	$\lambda_1 \approx 0.47595, \lambda_{2,3} \approx 0.00702 \pm 4.57910j$	Focus-Node Point (Unstable)	0.839
	$\mathcal{E}_2 = (0.10010; -0.20020; 0.20020)$	$\lambda_1 \approx -9.98800, \lambda_{2,3} \approx 0.24901 \pm 0.96808j$	Saddle-Focus Point (Unstable)	
Volta's System	$\mathcal{E}_1 = (0; 0; -1.3698)$	$\lambda_1 \approx 12.0299, \lambda_2 \approx -14.0299, \lambda_3 = -0.73$	Saddle Point (Unstable)	0.977
	$\mathcal{E}_2 = (-1.26310; -10.26032; -19.12310)$	$\lambda_1 = -2, \lambda_{2,3} \approx 0.3650 \pm 10.3313j$	Saddle-Focus Point (Unstable)	
	$\mathcal{E}_3 = (1.26310; 10.26032; -19.12310)$	$\lambda_1 \approx -7.2088, \lambda_2 \approx 7.93883, \lambda_3 = -2,$	Saddle Point (Unstable)	
Lü's System	$\mathcal{E}_1 = (0; 0; 0)$	$\lambda_1 = -3, \lambda_2 = 20, \lambda_3 = -36$	Saddle Point (Unstable)	0.9156
	$\mathcal{E}_2 = (7.7460; 7.7460; 20)$	$\lambda_1 \approx -22.6516, \lambda_{2,3} \approx 1.8258 \pm 13.6887j$	Saddle-Focus Point (Unstable)	
	$\mathcal{E}_3 = (-7.7460; -7.7460; 20)$	$\lambda_1 \approx -22.6516, \lambda_{2,3} \approx 1.8258 \pm 13.6887j$	Saddle-Focus Point (Unstable)	

pseudo-random sequences of 8-bit unsigned integers by using the following equation [23]:

$$X_j(ih) = \{\big(|x_j(ih)| - \lfloor x_j(ih)\rfloor\big) \times 10^{14}\} \,(\mathrm{mod}\,\mathcal{S});\quad \text{for}\, i = 0, 1, \ldots, \lfloor \tau_{sim}/h \rfloor;\quad j = 1, 2, \ldots, 9; \mathcal{S} = 2^k; 5 \le k \le 8 \tag{16}$$

where, $X_j(ih)$ denote the 8-bit pseudo-random integers corresponding to the 64-bit floating point values of $x_j(ih)$.

In this paper, a total of *nine* state-time histories corresponding to the fractional order Rössler's system, Volta's system, and Lü's system are used for generating *nine* different pseudo-random arrays of 8-bit unsigned integers, with the help of the concept presented in (16). These integers lie in the range [0, 2^k-1], and are almost uniformly distributed throughout the range with nearly zero correlation. Here, the initial conditions can be selected arbitrarily and a huge number of derivative orders can be chosen according to the stability conditions, given in (9) and (12). Hence, as many as 18 parameters (6 from each system) can influence the generation of nine pseudo-random sequences. A slight change in the control parameters will have significant impacts on the pseudo-random sequences thus generated, since the responses of the fractional order chaotic systems are highly sensitive to the initial conditions as well as the derivative orders.

However, with the aim to increase the degree of uniformity and independence, we propose the *multi-chaotic pseudo-random sequence generator* (MCPRSG), where the state-time histories from all the three FOCHS, after being converted to pseudo-random arrays, are combined in a novel, distinct manner. For this purpose, we consider three pseudo-random sequences of 8-bit unsigned integers, denoted as $\mathbf{Y}_1$, $\mathbf{Y}_2$, and $\mathbf{Y}_3$, each of which is a function of three chaotic state-time histories (one from each chaotic system). However, instead of allocating the chaotic states exactly in the same order every time (which means considering i^{th} states of all the three systems together, where $i = 1, 2, 3$), we propose to jumble up the state selections. The sequences $\mathbf{Y}_1$, $\mathbf{Y}_2$, and $\mathbf{Y}_3$ so generated are given as follows:

$$\mathbf{Y}_1 = \mathbf{X}_2 \oplus \mathbf{X}_4 \oplus \mathbf{X}_9,\quad \mathbf{Y}_2 = \mathbf{X}_3 \oplus \mathbf{X}_5 \oplus \mathbf{X}_7,\quad \mathbf{Y}_3 = \mathbf{X}_1 \oplus \mathbf{X}_6 \oplus \mathbf{X}_8. \tag{17}$$

As can be concluded from (17), each of $\mathbf{Y}_1$, $\mathbf{Y}_2$, and $\mathbf{Y}_3$ will get altered for different values of six control parameters (two from each system).

VI. STATISTICAL ANALYSIS OF THE PERFORMANCE OF THE PROPOSED PSEUDO-RANDOM SEQUENCE GENERATOR

In this section, we will compare efficiencies of our proposed MCPRSG and the MT-PRNG by conducting various statistical tests.

A. Chi-Square Test (χ^2)

The *Chi-square* test [25] is considered one of the most widely used statistical hypothesis tests, where we describe a test as "Chi-square" if the test statistic resulted is compared to a Chi square distribution with κ DOF (i.e. degrees of freedom); generally utilizing a Chi-squared distribution table or making use of the Chi-square distribution $\mathcal{R}$ function at a selected significance level. For the purpose of testing the qualities of the PRNGs, we use the Chi-square "goodness of fit" test which tests a hypothesis that a sample of observations follows a specified probability distribution. The method of testing simply considers the observations (i.e. the outputs) and the expectations (computed using probabilities from a proposed probability density function) of a PRNG to generate the result.

When hypothesis testing is done in association with "goodness of fit", we test a null hypothesis ($\mathcal{H}_0$) which normally represents the notion that the actual distribution of the sample being tested does not diverge significantly from the proposed distribution. Also, we define an alternative hypothesis ($\mathcal{H}_1$) which is based on the assumption that there is a significant difference between the expected distribution and the actual distribution. However, the level of significance ν is user defined. Formally, the hypotheses, for a random variable Z, may be defined as follows:

$$\mathcal{H}_0 : P(Z = j) = \mathfrak{p}_j \text{ for } j = 1, 2, \ldots, l.$$
$$\mathcal{H}_1 : Z \text{ has a different probability distribution.}$$

Now, the Chi-square test statistic is defined in the following form [25]:

$$\chi^2_\kappa = \sum_{j=1}^{l} \frac{(\mathcal{OB}_j - \mathcal{EX}_j)^2}{\mathcal{EX}_j} = \sum_{j=1}^{l} \frac{(\mathcal{OB}_j - \mathcal{L}\mathfrak{p}_j)^2}{\mathcal{L}\mathfrak{p}_j} \tag{18}$$

where, $\mathcal{OB}_j$ = the observed frequency of the j^{th} event, $\mathcal{EX}_j = \mathcal{L}\mathfrak{p}_j$ = the expected frequency of the j^{th} event under the statistical model proposed in $\mathcal{H}_0$, $\mathcal{L}$ = total count of events, and l = number of parameters.

After calculating χ^2_κ using (18), we compare the value with the values in a Chi-square distribution table. Such tables make use of DOF as a parameter to recognize which particular Chi-square distribution will be utilized to make comparison with the value. DOF is computed as: κ = no. of parameters-no. of constraints on the parameters. In our case, we consider $l-1$ DOF, since there are l parameters which are $\mathfrak{p}_1, \mathfrak{p}_2, \ldots \mathfrak{p}_l$, and only a single constraint is imposed on those parameters: $\mathfrak{p}_1 + \mathfrak{p}_2 \cdots + \mathfrak{p}_l = 1$.

Another outcome of the Chi-square test is the $\mathfrak{p}$-value. Note that, $\mathcal{H}_0$ assigns a probability framework against which we have to compare our observed data. Specifically, through the proposed model, $\mathcal{H}_0$ can be represented by a probability distribution which we call the $\mathfrak{p}$-value. The $\mathfrak{p}$-value provides the probabilities of all possible outcomes if $\mathcal{H}_0$ is true.

In our experiment, the proposed distribution is "uniform" distribution which means $\mathfrak{p}_1 = \mathfrak{p}_2 = \cdots = \mathfrak{p}_l$. We have considered pseudo random numbers in the range [0, 127]. Hence, total number of parameters $l = 128$, and accordingly $\kappa = 127$ (the constraint is $\mathfrak{p}_1 + \mathfrak{p}_2 \cdots + \mathfrak{p}_{128} = 1$). The total count of events $\mathcal{L}$ is considered to be 1500.

B. Kolmogorov-Smirnov Test

The Kolmogorov-Smirnov (K-S) test [25], a non-parametric test in nature, can also be employed as a "goodness of fit" test to evaluate the quality of a PRNG. However, being non-parametric, the K-S test does not make any assumption about the distribution of the samples under inspection. For testing PRNGs, we use the 'one-sample' K-S test so as to determine whether a sample comes from a proposed distribution or not.

The construction of the K-S test statistic is based on the cumulative distribution function (CDF) $\mathrm{F}_c(y)$. For a random variable Y, the CDF $\mathrm{F}_c(y)$ is defined as

$$\mathrm{F}_c(y) = P(Y \leq y)$$

The null hypothesis ($\mathcal{H}_0$) and the general alternative hypothesis ($\mathcal{H}_1$) for the one-sample K-S test tests are given as follows:

$\mathcal{H}_0$: The sample is drawn from a population following $\mathrm{F}_c(y)$.
$\mathcal{H}_1$: The sample is drawn from an another distribution.

The K-S test forms an "empirical" cumulative distribution based on observations and scans how much this distribution differs from a proposed distribution. Since the PRNGs are supposed to generate all the numbers with equal probability, the proposed distribution is the CDF $\mathrm{F}_c(y)$ for a Uniform distribution within the interval [0, 1], and will be considered as the base distribution with which we will compare our observed distribution.

Let us consider a sample of $\mathcal{L}$ independent observations O_1, O_2, ..., $O_\mathcal{L}$. Then, the empirical distribution function $\mathrm{F}_\mathcal{L}(y)$ is defined as [25]

$$\mathrm{F}_\mathcal{L}(y) = \frac{\sum_{j=1}^{\mathcal{L}} W[O_j \leq y]}{\mathcal{L}}; \text{ where } W[O_j \leq y] = \begin{cases} 1; & O_j \geq y \\ 0; & \text{else.} \end{cases}$$

The K-S test statistic determines the largest distance between $\mathrm{F}_\mathcal{L}(y)$ and $\mathrm{F}_c(y)$ and then compares this value to the values available in a K-S table. A good quality PRNG should be such that there will be a high degree of closeness between its empirical distribution function and the Uniform [0, 1] CDF, which means the largest distance between these two will be very small. However, we compute the largest distance between the two distributions with the help of two different statistics. One distance is calculated, considering that the empirical distribution is above the Uniform CDF and the other one is based on the consideration that the empirical distribution is below the Uniform CDF. The definitions of these two distances are formulated as [25]

$$\mathcal{K}^+_\mathcal{L} = \sqrt{\mathcal{L}} \max_{-\infty<y<\infty} (\mathrm{F}_\mathcal{L}(y) - \mathrm{F}_c(y))$$
$$\mathcal{K}^-_\mathcal{L} = \sqrt{\mathcal{L}} \max_{-\infty<y<\infty} (\mathrm{F}_c(y) - \mathrm{F}_\mathcal{L}(y))$$

The K-S test statistic, almost universally, is evaluated by means of the distance Δ, the largest between $\mathcal{K}^+_\mathcal{L}$ and $\mathcal{K}^-_\mathcal{L}$. The distance Δ is defined as [26]

$$\Delta = \max\left(\mathcal{K}^+_\mathcal{L}, \mathcal{K}^-_\mathcal{L}\right) = \max_{x\in\mathbb{R}} |\mathrm{F}_\mathcal{L}(y) - \mathrm{F}_c(y)| \tag{19}$$

C. Spearman's Rank Correlation Coefficient Test

Like K-S test, Spearman's Rank Correlation Coefficient (SRCC) test is also a non-parametric test [27], which is used to determine dependence between two variables. The SRCC test outputs a coefficient denoted as ρ which takes a value in the interval $[-1, 1]$.

Now, let us examine the quality of a PRNG which generates a pseudo-random sequence of size $\mathcal{L}$. We assume that the numbers generated from all odd iterations, S_1, S_3, ..., $S_{\mathcal{L}-1}$, follow a distribution P, whereas that from all even numbered iterations, S_2, S_4, ..., $S_\mathcal{L}$, follow a distribution Q. Here $\mathcal{L}$ is assumed to be an even number.

Each number from both P and Q is assigned a certain rank based on the comparisons of its numeric value and that of the remaining numbers in the respective distribution. The test statistic, in order to determine dependence between P and Q, utilizes the difference between ranks from P and Q. The null ($\mathcal{H}_0$) and the alternative ($\mathcal{H}_1$) hypotheses of the SRCC test are defined to be

$\mathcal{H}_0$: There is no correlation between P and Q.
$\mathcal{H}_1$: There is significant correlation between P and Q

The SRCC test statistic ρ is defined as [27]

$$\rho = \frac{\frac{2}{\mathcal{L}} \sum_{j=1}^{\frac{\mathcal{L}}{2}} \left(p_j - \bar{p}\right)\left(q_j - \bar{q}\right)}{\sqrt{\left(\frac{2}{\mathcal{L}} \sum_{j=1}^{\frac{\mathcal{L}}{2}} \left(p_j - \bar{p}\right)^2\right)\left(\frac{2}{\mathcal{L}} \sum_{j=1}^{\frac{\mathcal{L}}{2}} \left(q_j - \bar{q}\right)^2\right)}} \tag{20}$$

TABLE II
COMPARISON OF AVERAGE RESULTS OF VARIOUS STATISTICAL TESTS BETWEEN MCPRSG AND MT-PRNG. THE CRITICAL VALUES $\chi^2_{\kappa(\mathcal{C})}$, $\Delta_{(\mathcal{C})}$, AND $\mathcal{Z}_{s(\mathcal{C})}$ ARE CONSIDERED AT A LEVEL OF SIGNIFICANCE $\nu = 0.05$. WE FAIL TO REJECT $\mathcal{H}_0$ IF $\chi^2_{\kappa} < \chi^2_{\kappa(\mathcal{C})}$, $\Delta < \Delta_{(\mathcal{C})}$, $-\mathcal{Z}_{s(\mathcal{C})} < \mathcal{Z}_s < \mathcal{Z}_{s(\mathcal{C})}$, WHERE $\chi^2_{\kappa(\mathcal{C})} = 154.30$, $\Delta_{(\mathcal{C})} = \frac{1.36}{\sqrt{\mathcal{L}}} = 0.03512$, $\mathcal{Z}_{s(\mathcal{C})} = 1.96$. HERE, $\kappa = 127$, $\mathcal{L} = 1500$.

PRNG	Chi-Square Test		K-S Test	SRCC Test	
	χ^2_{κ}	p-value	Δ	ρ	$\mathcal{Z}_s$
MT-PRNG	132.37	0.4058	0.0334	0.0417	1.1076
MCPRSG	**110.06**	**0.7884**	**0.0143**	**0.0064**	**0.1698**

The test assesses how much the ranks of the j^{th} pairs, p_j and q_j, differ from each other. In case of PRNGs, this test is thus based on the correlation between pairs: $(p_1, q_1), \ldots, (p_{\frac{\mathcal{L}}{2}}, q_{\frac{\mathcal{L}}{2}})$ which denote the corresponding ranks of the consecutive pairs $(S_1, S_2), \ldots, (S_{\mathcal{L}-1}, S_{\mathcal{L}})$. Here, $\bar{p}$ and $\bar{q}$ indicate means of p_j and q_j (for $j = 1, 2, \ldots, \frac{\mathcal{L}}{2}$) respectively.

The sign of ρ indicates the direction in which P and Q are associated. If Q tends to increase when P increases, ρ is positive, whereas if Q tends to decrease when P increases, ρ is negative. A value of $\rho = 0$ indicates there is no monotonic relationship or no correlation between P and Q. The coefficient ρ measures how proficiently a monotonic function represents the relationship between P and Q, and hence, is competent to identify dependencies which the Pearson correlation coefficient cannot detect.

In order to determine whether an observed value of ρ significantly differs from zero, we can utilize the *Fisher transformation*, by means of which Spearman's coefficient value can be made comparable to the normal distribution. The Fisher transformation $\mathfrak{F}(\mathrm{r})$ of r (where, r is a correlation coefficient in the interval $[-1, 1]$) is defined as [28]

$$\mathfrak{F}(\mathrm{r}) = \frac{1}{2} \ln \frac{1+\mathrm{r}}{1-\mathrm{r}} = \tanh^{-1}(\mathrm{r}) \tag{21}$$

Considering ρ and $\mathcal{L}$ of SRCC test, the transformation $\mathfrak{F}(\mathrm{r})$ is normally distributed as follows [28]:

$$\mathfrak{F}(\mathrm{r}) \sim \mathcal{N}\left(\frac{1}{2} \ln \frac{1+\rho}{1-\rho}, \frac{1.06}{\mathfrak{n}-3}\right), \quad \text{where } \mathfrak{n} = \frac{\mathcal{L}}{2}$$

Let us consider a transformed version of $\mathfrak{F}(\mathrm{r})$, expressed as $\mathcal{Z}_s = \sqrt{\frac{\mathfrak{n}-3}{1.06}}\mathfrak{F}(\mathrm{r})$. It is mathematically confirmed that, under the null hypothesis of statistical independence ($\rho = 0$), $\mathcal{Z}_s$ will also follow the standard normal distribution, which means $\mathcal{Z}_s \sim \mathcal{N}(0, 1)$ [28].

Hence, after performing the previously defined transformation, we can now take help of a standard normal table to reach a definitive conclusion about whether or not there is significant dependence between two variables (i.e. consecutive pairs of outputs from a PRNG).

Table II shows the mean results obtained for both MCPRSG and MT-PRNG, when all the three above mentioned benchmark statistical tests were undertaken. The results obtained clearly demonstrate the superiority of MCPRSG over MT-PRNG, uniformly for all the three statistical tests. These results obtained for the benchmark tests encouraged us to implement the concept of MCPRSG based CBPICFAsT-match algorithm for the actual problem at hand i.e. real-life shoe detection for people following in a human robot coexisting environment.

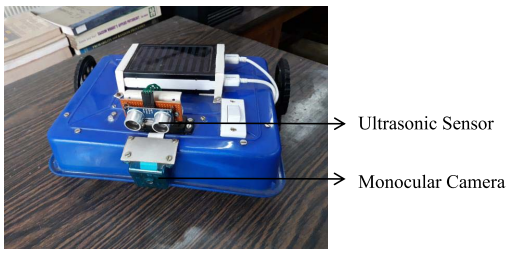

Fig. 2. The wheeled mobile robot used as the experimental platform.

(A) (B)

Fig. 3. (A) The matching image as well as the shoe template (*orange* bounding box) for $\mathcal{SQ}1$ and $\mathcal{SQ}2$, and (B) The matching image as well as the shoe template (*orange* bounding box) for $\mathcal{SQ}3$ and $\mathcal{SQ}4$.

VII. EXPERIMENTAL RESULTS

A. Experimental Setup

In this work, the experimental platform we utilize for evaluating the performance of our proposed CBPICFAsT-match algorithm is an indigenously developed, inexpensive wheeled mobile robot, depicted in Fig. 2, whose onboard processing unit is Raspberry Pi 3 model B+. This robot is an updated version of an earlier indigenously developed, inexpensive wheeled mobile robot utilized in [5]. A stationary monocular camera and an ultrasonic range finder (URF) are mounted on the robot for the purposes of sensing. The entire CBPICFAsT-match algorithm is implemented in `OpenCV-Python` in association with `Cython`.

The simulation parameters considered in the implementation of the CBPICFAsT-match algorithm are the same used in [5].

B. Performance Evaluations

We compare our proposed CBPICFAsT-match algorithm with the PICFAsT-match [5] and OBVTD [6] approaches, specifically developed for shoe detection purposes, as well as three other state-of-the-art visual target tracking algorithms of current interest, namely CSR-DCF [29], CCOT [30] and SCT [31]. Now, in order to assess the performance of CBPICFAsT-match qualitatively as well as quantitatively, we carry out experimental works on *four* image sequences, denoted as $\mathcal{SQ}1$, $\mathcal{SQ}2$, $\mathcal{SQ}3$, and $\mathcal{SQ}4$, the frames of which are captured by the onboard monocular camera of the wheeled mobile robot in Fig. 2, during pursuit in various laboratory environments considerably affected by different photometric variations, such as illumination, shadows, specularities etc. Apart from the photometric changes, $\mathcal{SQ}1$, $\mathcal{SQ}2$, $\mathcal{SQ}3$, and $\mathcal{SQ}4$ experience various other challenging difficulties, for

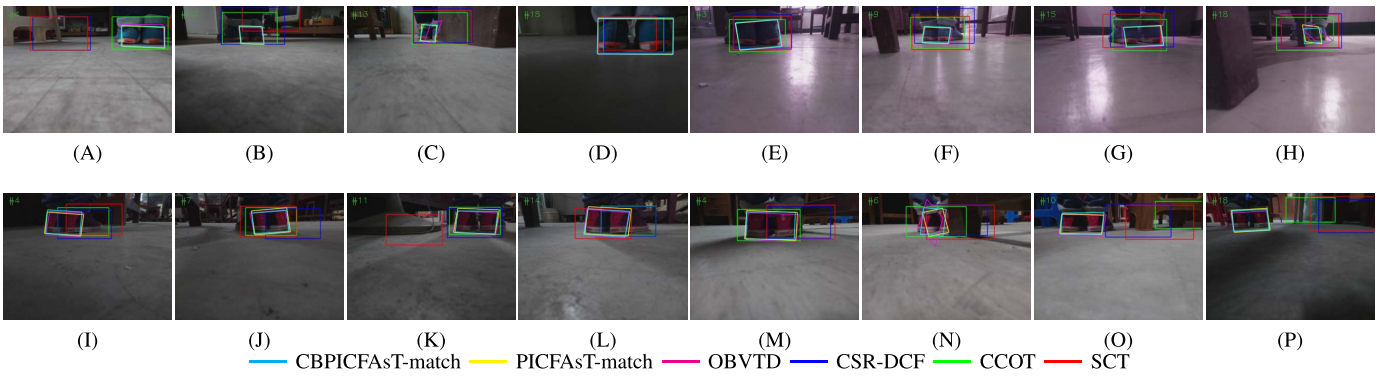

Fig. 4. Qualitative comparisons among the competing algorithms in terms of the tracking outcomes (bounding quadrilaterals) of some representative frames of $\mathcal{SQ}1$ (A-D), $\mathcal{SQ}2$ (E-H), $\mathcal{SQ}3$ (I-L), and $\mathcal{SQ}4$ (M-P).

instance, improper brightnesses and contrasts, scale variations, rotations, background clutters, partial occlusions, etc. Fig. 3 shows the reference frames (matching images) corresponding to $\mathcal{SQ}1$, $\mathcal{SQ}2$, $\mathcal{SQ}3$, and $\mathcal{SQ}4$, as well as the templates of shoes automatically determined from the frames.

The results of qualitative evaluation for some representative frames of $\mathcal{SQ}1$, $\mathcal{SQ}2$, $\mathcal{SQ}3$, and $\mathcal{SQ}4$ are shown in Fig. 4 which depict the visual object tracking outcomes for the competing algorithms. As we can see in Fig. 4, despite the aforementioned challenges (excluding partial occlusions), CBPICFAsT-match succeeds to precisely identify the target shoes in various frames of $\mathcal{SQ}1$, $\mathcal{SQ}2$, $\mathcal{SQ}3$, and $\mathcal{SQ}4$.

For the purpose of evaluating the tracking algorithms quantitatively, we utilize *six* performance metrics, namely *center location error* (CLE) [32], *root-mean-square-error* (RMSE) [33], *overlap ratio* (OR) [32], *combined tracking performance score* (CoTPS) [33], *distance precision* (DP) [32], and *overlap precision* (OP) [32]. Table III reports the mean CLE, RMSE, OR, CoTPS, DP, OP and Frame per second (FPS) count values of the competing tracking algorithms on the image sequences $\mathcal{SQ}1$, $\mathcal{SQ}2$, $\mathcal{SQ}3$, and $\mathcal{SQ}4$. As can be seen from the comparison results in Table III, the proposed CBPICFAsT-match improves the overall matching results compared to our earlier proposed PICFAsT-match and OBVTD algorithms, while significantly outperforming the remaining three tracking algorithms. From Table III we note as well that the mean speed of CSR-DCF tracking algorithm is a bit higher than the rest five algorithms. From this viewpoint, our CBPICFAsT-match algorithm appears to be somewhat slower, since the approach, like PICFAsT-match and OBVTD algorithms, searches the space of 2D affine transformations for determining the optimal (affine) transformation corresponding to each frame. However, Table III evidences the superiority of the CBPICFAsT-match algorithm over the remaining five algorithms in terms of the quantitative metrics, which inevitably makes the approach a preferred option among the state-of-the-art choices available. Fig. 5 depicts the average *precision* and *success* plots of one-pass evaluation (OPE) [32] for the competing algorithms on four sequences, which also reveals that the proposed CBPICFAsT-match ranks supreme among the six algorithms.

In this context, it is worth mentioning that OBVTD can be considered as almost a general-purpose template matching

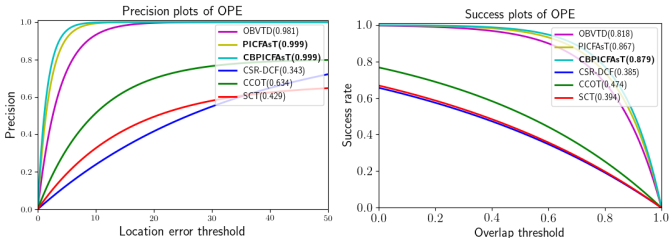

Fig. 5. Average precision and success plots: the legend of the precision plot denotes the average DP score at 15 pixels for each competing algorithm, and the legend of the success plot indicates the normalized-area-under-the curve (NAUC) value for each competing algorithm.

TABLE III
COMPARISONS OF AVERAGE PERFORMANCE METRICS FOR THE COMPETING ALGORITHMS

Algorithms	CLE	RMSE	OR	CoTPS	DP (%)	OP (%)	FPS Count
OBVTD	4.11	5.47	0.809	0.191	92.54	82.31	1.25
PICFAsT-match	2.48	3.31	0.869	0.131	95.73	86.68	1.11
CBPICFAsT-match	**2.17**	**2.95**	**0.880**	**0.120**	**96.44**	**88.37**	1.08
CSR-DCF	38.35	59.42	0.355	0.535	34.41	28.34	**7.95**
CCOT	25.69	48.92	0.454	0.456	63.24	36.43	0.09
SCT	41.25	64.17	0.367	0.459	42.52	29.15	1.59

algorithm which performs successfully in a wide range of challenging real-life environments including the photometrically affected scenarios, especially where the clustering performances of DBSCAN are quite unsatisfactory. On the other hand, CBPICFAsT-match and PICFAsT-match are specifically developed to deal with the environments significantly affected with various photometric variations. Hence, it is pretty justified that, for the photometrically affected frames considered in this work, the matching results obtained with CBPICFAsT-match and PICFAsT-match are uniformly better than those obtained with OBVTD, which is evidenced by Table III, Fig. 4 and Fig. 5.

VIII. CONCLUSION

The present paper proposes an improved version of PICFAsT-match, called *chaos based PICFAsT-match (CBPICFAsT-match)*, a novel solution for shoe detection based people following in human-robot coexisting photometrically challenged environments, which accomplishes

random sampling of image pixels based on *multi-chaotic pseudo-random sequence generator (MCPRSG)*. The paper first demonstrates how a greater degree of uniformity and independence can be achieved with the newly proposed MCPRSG based pseudo-random sequences in comparison to that generated with Python's *Mersenne-Twister* (MT)-PRNG. Then the proposed MCPRSG is utilized to develop our novel proposal of *CBPICFAsT-match* algorithm. The supremacy of CBPICFAsT-match is experimentally illustrated, in comparison to the earlier proposed PICFAsT-match and OBVTD, as well as some other state-of-the-art tracking algorithms of current interest.

REFERENCES

[1] H.-M. Gross *et al.*, "Mobile robotic rehabilitation assistant for walking and orientation training of stroke patients: A report on work in progress," in *Proc. IEEE Int. Conf. Syst. Man Cybern. (SMC)*, San Diego, CA, USA, Oct. 2014, pp. 1880–1887.

[2] H. Wang and X. P. Liu, "Adaptive shared control for a novel mobile assistive robot," *IEEE/ASME Trans. Mechatronics*, vol. 19, no. 6, pp. 1725–1736, Dec. 2014.

[3] J. Yuan, H. Chen, F. Sun, and Y. Huang, "Multisensor information fusion for people tracking with a mobile robot: A particle filtering approach," *IEEE Trans. Instrum. Meas.*, vol. 64, no. 9, pp. 2427–2442, Sep. 2015.

[4] N. Bellotto and H. Hu, "Multisensor-based human detection and tracking for mobile service robots," *IEEE Trans. Syst. Man, Cybern. B, Cybern.*, vol. 39, no. 1, pp. 167–181, Feb. 2009.

[5] P. Paral, A. Chatterjee, and A. Rakshit, "Vision sensor-based shoe detection for human tracking in a human–robot coexisting environment: A photometric invariant approach using DBSCAN algorithm," *IEEE Sensors J.*, vol. 19, no. 12, pp. 4549–4559, Jun. 2019.

[6] P. Paral, A. Chatterjee, and A. Rakshit, "OPTICS-based template matching for vision sensor-based shoe detection in human–robot coexisting environments," *IEEE Trans. Instrum. Meas.*, vol. 68, no. 11, pp. 4276–4284, Nov. 2019.

[7] Y. Lu and S. Velipasalar, "Autonomous footstep counting and traveled distance calculation by mobile devices incorporating camera and accelerometer data," *IEEE Sensors J.*, vol. 17, no. 21, pp. 7157–7166, Nov. 2017.

[8] K. Ozcan and S. Velipasalar, "Robust and reliable step counting by mobile phone cameras," in *Proc. 9th Int. Conf. Dist. Smart Cameras*, New York, NY, USA, Sep. 2015, pp. 164–169.

[9] S. Korman, D. Reichman, G. Tsur, and S. Avidan, "Fast-match: Fast affine template matching," in *Proc. IEEE Conf. Comput. Vis.Pattern Recog. (CVPR)*, Portland, OR, USA, Jun. 2013, pp. 2331–2338.

[10] D. Jia, X.-L. Tang, H. Zhu, J. Cao, and W.-D. Song, "Colour FAST (CFAST) match: Fast affine template matching for colour images," *Electron. Lett.*, vol. 52, no. 14, pp. 1220–1221, Jul. 2016.

[11] M. Ester, H.-P. Kriegel, J. Sander, and X. Xu, "A density-based algorithm for discovering clusters in large spatial databases with noise," in *Proc. 2nd Int. Conf. Knowl. Discovery Data Mining*, Portland, OR, USA, 1996, pp. 226–231.

[12] M. Ankerst, M. Breunig, H.-P. Kreigel, and J. Sander, "OPTICS: Ordering points to identify the clustering structure," in *Proc. ACM SIGMOD Int. Conf. Manage. Data*, Philadelphia, PA, USA, Jun. 1999, pp. 49–60.

[13] S. Raskhodnikova, "Approximate testing of visual properties," in *Proc. 7th Int. Workshop Randomization Approximation Techn. Comput. Sci.*, Princeton, NJ, USA, Aug. 2003, pp. 370–381.

[14] *Python 2.7.16 Documentation Webpage*. Accessed: Sep. 30, 2019. [Online]. Available: https://docs.python.org/2.7/

[15] I. Petráš, *Fractional-Order Nonlinear Systems: Modeling, Analysis and Simulation*. Berlin, Germany: Springer-Verlag, 2011, pp. 184–187.

[16] S. Oishi and H. Inoue, "Pseudo-random number generators and chaos," *Trans. Inst. Electron. Commun. Eng. Jpn. E*, vol. 65, no. 1, pp. 534–541, Sep. 1982.

[17] S. W. Golomb, *Shift Register Sequences*. San Francisco, CA, USA: Holden-Day, 1967.

[18] N. Kalouptsidis, *Signal Processing Systems: Theory and Design*. New York, NY, USA: Wiley, 1997.

[19] F. Sun, S. Liu, Z. Li, and Z. Lü, "A novel image encryption scheme based on spatial chaos map," *Chaos, Solitons Fractals*, vol. 38, no. 3, pp. 631–640, Nov. 2008.

[20] X. Tong and M. Cui, "Image encryption with compound chaotic sequence cipher shifting dynamically," *Image Vis. Comput.*, vol. 26, no. 6, pp. 843–850, Jun. 2008.

[21] K. B. Oldham and J. Spanier, *The Fractional Calculus: Theory and Applications of Differentiation and Integration to Arbitrary Order*. New York, NY, USA: Dover, 2002.

[22] A. G. Radwan, S. K. Abd-El-Hafiz, and S. H. AbdElHaleem, "Image encryption in the fractional-order domain," in *Proc. Int. Conf. Eng. Technol.*, Cairo, Egypt, Oct. 2012, pp. 1–6.

[23] P. Paral, T. Dasgupta, and S. Bhattacharya, "Colour image encryption based on cross-coupled chaotic map and fractional order chaotic systems," in *Proc. Int. Conf. Commun. Sign. Process.*, Melmaruvathur, India, Apr. 2014, pp. 1947–1952.

[24] W. Deng, "Short memory principle and a predictor–corrector approach for fractional differential equations," *J. Comput. Appl. Math.*, vol. 206, no. 1, pp. 174–188, Sep. 2007.

[25] D. E. Knuth, "Random numbers," in *The Art of Computer Programming*, vol. 2. Reading, MA, USA: Addison-Wesley, 1969, pp. 37–44.

[26] M. Hollander and D. A. Wolfe, *Nonparametric Statistical Methods*. New York, NY, USA: Wiley, 1973, p. 226.

[27] T. Cleff, *Exploratory Data Analysis in Business and Economics: An Introduction Using SPSS, Stata, and Excel*. Berlin, Germany: Springer, 2014.

[28] E. C. Fieller and E. S. Pearson, "Tests for rank correlation coefficients: II," *Biometrika*, vol. 48, nos. 1–2, pp. 29–40, Jun. 1961.

[29] A. Lukežič, T. Vojíř, L. Č. Zajc, J. Matas, and M. Kristan, "Discriminative correlation filter with channel and spatial reliability," in *Proc. IEEE Conf. Comput. Vis. Pattern Recognit. (CVPR)*, Honolulu, HI, USA, Jul. 2017, pp. 4847–4856.

[30] M. Danelljan, A. Robinson, F. Shahbaz Khan, and M. Felsberg, "Beyond correlation filters: Learning continuous convolution operators for visual tracking," in *Proc. Eur. Conf. Comput. Vis. (ECCV)*, Amsterdam, The Netherlands, Oct. 2016, pp. 472–488.

[31] J. Choi, H. J. Chang, J. Jeong, Y. Demiris, and J. Y. Choi, "Visual tracking using attention-modulated disintegration and integration," in *Proc. IEEE Conf. Comput. Vis. Pattern Recognit. (CVPR)*, Las Vegas, NV, USA, Jun. 2016, pp. 4321–4330.

[32] R. Yao, S. Xia, F. Shen, Y. Zhou, and Q. Niu, "Exploiting spatial structure from parts for adaptive kernelized correlation filter tracker," *IEEE Signal Process. Lett.*, vol. 23, no. 5, pp. 658–662, May 2016.

[33] L. Čehovin, A. Leonardis, and M. Kristan, "Visual object tracking performance measures revisited," *IEEE Trans. Image Process.*, vol. 25, no. 3, pp. 1261–1274, Mar. 2016.